

Ultrasmall PEGylated $\text{Mn}_x\text{Fe}_{3-x}\text{O}_4$ ($x = 0-0.34$) nanoparticles: effects of Mn(II) doping on T_1 - and T_2 -weighted magnetic resonance imaging†

Cite this: *RSC Adv.*, 2013, **3**, 23454

Lijing Wang,^a Qiong Wu,^a Su Tang,^a Jianfeng Zeng,^b Ruirui Qiao,^b Pan Zhao,^a Yuan Zhang,^a Fengqin Hu^{*a} and Mingyuan Gao^b

We report a facile synthesis of water-soluble, ultrasmall, PEGylated $\text{Mn}_x\text{Fe}_{3-x}\text{O}_4$ nanoparticles (MFNPs) ($x = 0-0.34$) and the Mn(II) doping effects on T_1 - and T_2 -weighted magnetic resonance imaging (MRI). By adjusting the reaction conditions, the 'x' value can be continuously tuned from 0 to 0.34. The produced MFNPs are of high crystallinity and size uniformity with an average diameter of ~6 nm, which show excellent colloidal stability in H_2O , PBS, and tolerate a high salt concentration (1 M NaCl) and a wide pH range from 7 to 11. The results of FTIR demonstrate that both HOOC-PEG-COOH and TEG were modified on the nanocrystal surfaces. The saturation magnetization of the MFNPs gradually increases with increasing Mn^{2+} concentration and reaches 75.5 emu g^{-1} for $x = 0.34$. Careful investigation of the Mn(II) doping effects on T_1 - and T_2 -weighted MRI reveals that T_2 contrast effects are enhanced while T_1 contrast effects are weakened with the increase of the 'x' value of the MFNPs. Furthermore, the T_1 contrast effects of the MFNPs are concentration dependant. A concentration which is lower than 0.500 mM is needed for the MFNPs to act as T_1 and T_2 dual contrast agents at 3 T.

Received 29th July 2013
Accepted 1st October 2013

DOI: 10.1039/c3ra43985b

www.rsc.org/advances

1. Introduction

Magnetic resonance imaging (MRI) is among the best noninvasive methodologies today in clinical medicine for assessing anatomy and function of tissues. The MRI technique offers several advantages such as excellent temporal and spatial resolution, the lack of exposure to radiation, rapid *in vivo* acquisition of images, and long effective imaging window.¹⁻⁵ However, MRI is much less sensitive than nuclear medicine or fluorescence imaging when used to monitor small tissue lesions, molecular activity, or cellular activities.^{1,4,6} Therefore, searching for ultrasensitive contrast agents has drawn a lot of attention during the last decade.

Compared with the conventional paramagnetic agents, nanoparticle-based contrast agents have a number of advantages due to their nanoparticulate structures: (1) the magnetic properties of the agents can be tailored by size, shape, composition and assembly; (2) the nanoparticulate agents show tunable cellular uptake; (3) the agents have large specific surface areas that facilitate conjugation with targeting

molecules and other probes for achieving targeting and multi-modal agents, and (4) the nanoscale dimension, adjustable surface structure and shape of the agents allow varying and favorable biodistribution. Among the different kinds of magnetic nanoparticle contrast agents, magnetite (Fe_3O_4) nanoparticles (NPs) are the most widely studied for their high saturation magnetization and biocompatibility.⁷⁻¹¹ Recently, $\text{M}_x\text{Fe}_{3-x}\text{O}_4$ ($\text{M} = \text{Mn}, \text{Co}, \text{Ni}, \text{Zn}, 0 < x \leq 1$) NPs were demonstrated as potential MR contrast agents as the magnetic configurations of the NPs can be molecularly engineered to provide a wide range of magnetic properties by adjusting the chemical identity and the M^{2+} doping level.¹²⁻¹⁶ Among these ferrite NPs, $\text{Mn}_x\text{Fe}_{3-x}\text{O}_4$ NPs (MFNPs) have been proved to be a good candidate as they have higher magnetization than magnetite NPs and other metal-doped iron oxide NPs such as cobalt ferrite and nickel ferrite. More importantly, MFNPs have stronger MR contrast effect than magnetite NPs in T_2 -weighted images with much higher transverse relaxivity.^{14,17} However, for T_2 MR contrast applications, their negative contrast effect and magnetic susceptibility artifacts sometimes might induce false diagnosis. Therefore, the development of T_1 or $T_1 + T_2$ dual-contrast MR contrast agents based on magnetic nanoparticles has become a hot topic.¹⁸⁻²⁷ To the best of our knowledge, there are few reports on the T_1 contrast effects of the MFNPs.^{28,29} Systematic investigation of T_1 contrast effects of the MFNPs and evaluation of their performance as $T_1 + T_2$ dual-contrast MR contrast agents are desired.

^aCollege of Chemistry, Beijing Normal University, Beijing 100875, People's Republic of China. E-mail: fqhu@bnu.edu.cn

^bInstitute of Chemistry, CAS, Bei Yi Jie 2, Beijing 100190, People's Republic of China

† Electronic Supplementary Information (ESI) available: Fig. S1: TEM result of the $\text{Mn}_{0.30}\text{Fe}_{2.70}\text{O}_4$ NPs; Fig. S2: DLS result of the $\text{Mn}_{0.34}\text{Fe}_{2.66}\text{O}_4$ NPs freshly dispersed in PBS; Fig. S3: thermal gravimetric analysis (TGA) result of the $\text{Mn}_{0.34}\text{Fe}_{2.66}\text{O}_4$ NPs. See DOI: 10.1039/c3ra43985b

Thermal decomposition has been considered as one of the most effective methods for the synthesis of MFNPs.^{12,14,30,31} Sun *et al.* developed a convenient organic phase process of making monodisperse MFNPs through the reaction of $\text{Fe}(\text{acac})_3$ and $\text{Mn}(\text{acac})_2$, with 1,2-hexadecanediol in the presence of oleic acid and oleylamine.¹² To make the as-prepared MFNPs water-soluble, sophisticated post-preparative processes have been adopted. For example, Weller and coworkers reported three different approaches, including ligand exchange of oleic acid using water-soluble polymer, coating of individual MFNPs with amphiphilic polymer, and embedding the MFNPs into lipid micelles, to achieve the water solubility of the MFNPs.³² Up to present, there are still several obstacles for the preparation of high quality MFNPs. First, most of the MFNPs prepared by this approach are only soluble in organic solvents, thereby limiting their biological applications. In this case, sophisticated post-preparative processes have been devoted to making the particles water-soluble and biocompatible.^{32–34} However, these processes, in some cases, could significantly increase the overall size of the MFNPs, leading to limited tissue distribution, penetration, and metabolic clearance of the MFNPs.³⁵ Second, the molar ratio between manganese and iron, *i.e.*, the 'x' value in the MFNPs, is difficult to control through varying the ratio of initial precursors. $\text{Fe}(\text{acac})_3$ [iron(III) acetylacetonate] and $\text{Mn}(\text{acac})_2$ [manganese(II) acetylacetonate] are generally used as metal precursors in the preparation of MFNPs. The thermal decomposition temperatures of $\text{Fe}(\text{acac})_3$ and $\text{Mn}(\text{acac})_2$ are 186 °C and 249 °C, respectively.³⁶ The huge difference between the decomposition temperatures makes it difficult to precisely control the chemical composition of the MFNPs.^{32,36,37}

In this paper, we report a facile one-pot reaction to synthesize monodisperse, water-soluble, ultrasmall (~6 nm) MFNPs with excellent colloidal stability. The effects of preparation conditions (reaction time, metal precursor concentration, and heating procedure) on 'x' values were investigated, and the 'x' values were successfully tuned from 0 to 0.34 by adjusting the conditions. The Mn^{2+} doping effect on r_1 and r_2 , T_1 and T_2 MR contrast effects was also investigated. MR phantom experiments demonstrated that the T_1 contrast effects of the MFNPs are concentration dependent due to their high T_2 contrast effects. As the Fe + Mn concentration of the MFNPs is lower than 0.500 mM, they present good T_1 and T_2 dual modal MR contrast effects at a magnetic field strength of 3 T.

2. Experimental details

2.1 Synthesis of the MFNPs

MFNPs were prepared through modifying the procedure we have developed for the synthesis of high-quality Fe_3O_4 NPs.¹⁹ A typical synthesis to produce $\text{Mn}_{0.24}\text{Fe}_{2.76}\text{O}_4$ NPs is as follows: 2 mmol $\text{Fe}(\text{acac})_3$ (99.9+%, Aldrich), 1 mmol $\text{Mn}(\text{acac})_2$ (Aldrich), 6 g HOOC-PEG-COOH [poly(ethylene glycol) bis(carboxymethyl) ether, Aldrich, 600 g mol⁻¹] and 25 ml TEG [tetra(ethylene glycol), 99%, Aldrich] were mixed and purged with nitrogen. The reaction mixture was magnetically stirred at ~100 °C until all of the reagents were completely dissolved into the solvent. Then, the mixture was heated to 210 °C and kept for

2 h. Afterwards, the reaction solution was heated to reflux (~287 °C) and kept at that temperature for 1 h. The preparation of $\text{Mn}_{0.22}\text{Fe}_{2.78}\text{O}_4$ and $\text{Mn}_{0.26}\text{Fe}_{2.74}\text{O}_4$ NPs was similar to that of $\text{Mn}_{0.24}\text{Fe}_{2.76}\text{O}_4$ NPs except that the reaction time at ~287 °C is different: 0.5 h for $\text{Mn}_{0.22}\text{Fe}_{2.78}\text{O}_4$ NPs; 2 h for $\text{Mn}_{0.26}\text{Fe}_{2.74}\text{O}_4$ NPs. The synthesis of $\text{Mn}_{0.29}\text{Fe}_{2.71}\text{O}_4$ NPs is similar to that of $\text{Mn}_{0.26}\text{Fe}_{2.74}\text{O}_4$ NPs except that 2 mmol $\text{Mn}(\text{acac})_2$ were added.

The $\text{Mn}_{0.34}\text{Fe}_{2.66}\text{O}_4$ NPs was prepared through a slightly modified procedure: 2 mmol $\text{Fe}(\text{acac})_3$, 1 mmol $\text{Mn}(\text{acac})_2$, 6 g HOOC-PEG-COOH and 25 ml TEG were mixed and purged with nitrogen. After all of the reagents were completely dissolved into the solvent, the reaction mixture was heated to reflux (~287 °C) and kept at that temperature for 2 h. The preparation of Fe_3O_4 , $\text{Mn}_{0.13}\text{Fe}_{2.87}\text{O}_4$, and $\text{Mn}_{0.25}\text{Fe}_{2.75}\text{O}_4$ NPs was similar to that of $\text{Mn}_{0.34}\text{Fe}_{2.66}\text{O}_4$ NPs except that different amounts of $\text{Mn}(\text{acac})_2$ were used: 0 mmol $\text{Mn}(\text{acac})_2$ for Fe_3O_4 NPs, 0.125 mmol $\text{Mn}(\text{acac})_2$ for $\text{Mn}_{0.13}\text{Fe}_{2.87}\text{O}_4$ NPs; 0.500 mmol $\text{Mn}(\text{acac})_2$ for $\text{Mn}_{0.25}\text{Fe}_{2.75}\text{O}_4$ NPs.

A hot injection procedure was adopted in the synthesis of $\text{Mn}_{0.30}\text{Fe}_{2.70}\text{O}_4$ NPs. A solution of 6 g HOOC-PEG-COOH in 20 ml TEG was degassed and heated to 260 °C under stirring. Subsequently, a 100 °C solution of 1 mmol $\text{Mn}(\text{acac})_2$ and 2 mmol $\text{Fe}(\text{acac})_3$ in 5 ml TEG (also heated under nitrogen) was injected. The mixture was then heated to reflux at ~287 °C for 2 h.

All of the reaction solutions were treated through two ways: an aqueous solution of the NPs was obtained through dialyzing the reaction solution against 0.1 M sodium citrate for 2 days to remove all species with molecular weights smaller than 8000; a powder sample was obtained by collecting the NPs through centrifugation of the reaction solution at 13 200 rpm for 60 min, washing with double-distilled water and ethanol for three times respectively, and then drying at room temperature.

2.2 Characterization

TEM image and selected-area electron diffraction patterns were obtained on a JEM-100CX II electron microscope operating at an acceleration voltage of 100 kV. Samples for TEM were prepared by spreading a drop of the solution sample on copper grids coated with a carbon film followed by evaporation under ambient conditions. The nanoparticle diameters were determined by statistical averaging through calculating 200 nanoparticles. The iron and manganese concentrations of each NP sample were determined by inductively coupled plasma optical emission spectroscopy (ICP-OES, Thermo Fisher, iCAP6000). Prior to ICP measurements, the NP samples were digested in 69% nitric acid at room temperature overnight and diluted to 3% (v/v) nitric acid. DLS measurements were performed with a Malvern Instrument Zetasizer Nano Series Nano-ZS. XRD measurements were carried out on a powder sample of the NPs using a Philips X'pert ProMPD diffractometer with Cu-K α radiation. FTIR spectra were obtained with a Nicolet 380 Fourier transform infrared spectrometer. Room temperature magnetization was measured on a homemade vibrating sample magnetometer. Longitudinal and transverse relaxation times were measured at 1.5 T (60 MHz) and 37 °C on a Bruker mq60 NMR Analyzer. An inversion–recovery pulse sequence was used

to measure the longitudinal relaxation times and a spin echo pulse sequence was used to measure the transverse relaxation times. MR phantom images were acquired on a Philips 3.0 T TX clinical imaging system at ambient temperature (~ 25 °C). A T_1 -weighted image was acquired using a SE pulse sequence with TR = 500 ms, TE = 12 ms, FOV = 170×170 mm², data matrix = 640×640 and slice thickness = 6 mm. A T_2 -weighted image was acquired using a TSE pulse sequence with TSE factor = 15, TR = 2500 ms, TE = 90 ms, FOV = 175×175 mm², data matrix = 704×704 and slice thickness = 3 mm. T_1 was measured using a MIX pulse sequence with TR-SE = 920 ms, TR-IR = 2300 ms, TI = 500 ms, FOV = 170×170 mm², data matrix = 512×512 and slice thickness = 6 mm. T_2 was measured using a SE multi-echo pulse sequence with TR = 500 ms, 16 echoes with 12.25 ms even echo space, FOV = 180×180 mm², data matrix = 480×480 and slice thickness = 6 mm.

3. Results and discussion

A polyol process was designed to synthesize MFNPs by using Fe(acac)₃ and Mn(acac)₂ as metal precursors, HOOC-PEG-COOH as stabilizer and TEG as solvent. Fig. 1(a) shows the representative TEM image of the Mn_{0.24}Fe_{2.76}O₄ NPs. The average NP size is 6.4 nm. A standard deviation of 0.46 nm demonstrates their high monodispersity. Selected-area electron diffraction patterns shown in Fig. 1(c) reveal that the Mn_{0.24}Fe_{2.76}O₄ NPs are of high crystallinity. The ratio of Mn/Fe in Mn_{0.24}Fe_{2.76}O₄ NPs is 0.0869, which is much less than that of initial Mn(acac)₂ to Fe(acac)₃ precursors (0.5). Similar results have been reported before.^{32,36}

The Mn²⁺ doping level could be effectively controlled by changing the preparation conditions. The results in Table 1 reveal that the primary factors that influence 'x' value are reaction time, metal precursor concentration, and heating procedure. As the amounts of Mn(acac)₂ and Fe(acac)₃ were fixed, extending reaction time resulted in high 'x' value. From No. 1 to No. 3, the reaction time at ~ 287 °C increased from 0.5 h to 2 h, the 'x' increased from 0.22 to 0.26 accordingly. Since the colloidal stability of the MFNPs synthesized after 2 h drastically decreased, the optimal reaction time is 2 h. High Mn(acac)₂ to Fe(acac)₃ ratio also resulted in high 'x' value, which can be observed from no. 6 to no. 9.

Besides reaction time and metal precursor concentration, heating procedure also has great influence on 'x' value. Compared with the procedure in which the reaction mixture was heated to 210 °C first and then to reflux, direct heating of the solution to reflux resulted in MFNPs with higher 'x' value. For example, as 1 mmol Mn(acac)₂ and 2 mmol Fe(acac)₃ were used as precursors, the 'x' value of the obtained MFNPs through the direct heating procedure is 0.34, which is 31% higher than that of the MFNPs prepared through stepwise heating. As described in the introduction section, there is a huge difference between the thermal decomposition temperatures of Fe(acac)₃ (186 °C) and Mn(acac)₂ (249 °C). Direct heating procedure could shorten the time difference between the initial decomposition of the two precursors, and thus resulting in high Mn²⁺ doping level.

To further shorten the time difference between the initial decomposition of Mn(acac)₂ and Fe(acac)₃, we developed a hot injection method. Mn(acac)₂ and Fe(acac)₃ were injected into a hot TEG solution (260 °C) containing HOOC-PEG-COOH, which was then heated to reflux and kept for 2 h. ICP-OES revealed that the 'x' value of the MFNPs through this procedure is 0.30, which is lower than that (0.34) of the MFNPs synthesized through the direct heating procedure. The hot injection resulted in burst nucleation and rapid growth, and thus there was not enough time for more Mn²⁺ ions to dope into the crystal lattice of the Fe₃O₄ NPs. Fig. S1† shows the TEM image and selected-area electron diffraction patterns of the Mn_{0.30}Fe_{2.70}O₄ NPs. The average NP size is 6.2 nm with a standard deviation of 0.65 nm. The size of the Mn_{0.30}Fe_{2.70}O₄ NPs is similar to that shown in Fig. 1, while the monodispersity is not as good as the NPs synthesized through thermal decomposition. It is worth noting that the size of all of the MFNPs described above is ~ 6 nm.

Powder X-ray diffraction (XRD) was performed to examine the crystal structure of the MFNPs. As shown in Fig. 2, the diffraction peaks of MnFe₂O₄ and Fe₃O₄ are similar, especially at low angles. The diffraction peaks of MnFe₂O₄ shift to lower angles compared to those of Fe₃O₄. The position of the diffraction peaks of the Mn_{0.34}Fe_{2.66}O₄ NPs mostly matches with those for magnetite. This attributes to the low Mn²⁺ doping amount and has already been shown.^{14,38} The average crystallite size calculated from the (311) diffraction peak using the Scherrer equation was about 6.3 nm, which is consistent with that observed by TEM.

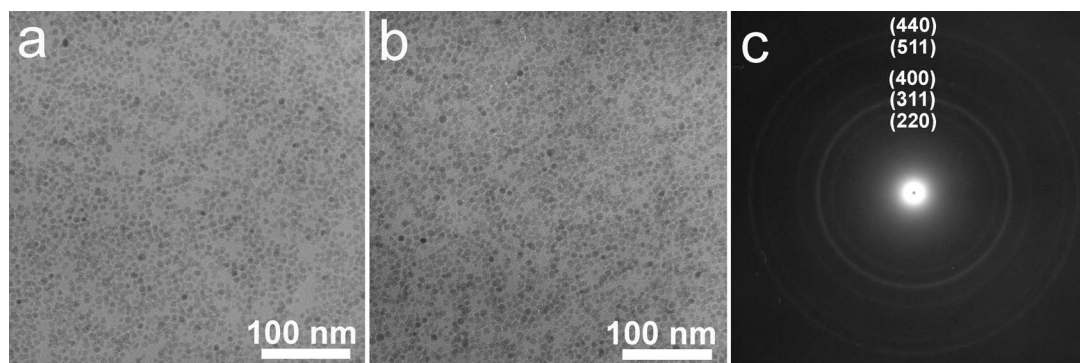
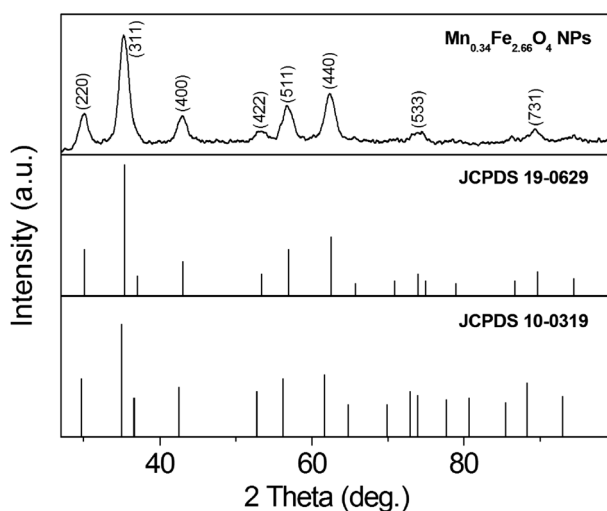


Fig. 1 TEM images of (a) the Mn_{0.24}Fe_{2.76}O₄ and (b) Mn_{0.34}Fe_{2.66}O₄ NPs. (c) Electron diffraction patterns of the Mn_{0.24}Fe_{2.76}O₄ NPs.

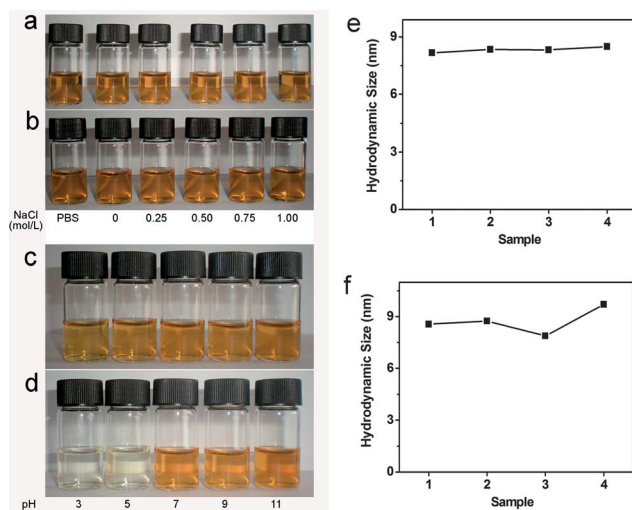
Table 1 Effects of the reaction conditions on Mn²⁺ doping level

No.	Mn(acac) ₂ (mmol)	Fe(acac) ₃ (mmol)	Reaction condition	Mn/Fe	x
1	1.000	2.000	210 °C for 2 h; ~287 °C for 0.5 h	0.0791	0.22
2	1.000	2.000	210 °C for 2 h; ~287 °C for 1 h	0.0869	0.24
3	1.000	2.000	210 °C for 2 h; ~287 °C for 2 h	0.0953	0.26
4	2.000	2.000	210 °C for 2 h; ~287 °C for 2 h	0.1070	0.29
5	1.000	2.000	Hot injection	0.1101	0.30
6	0.000	2.000	~287 °C for 2 h	0.0000	0.00
7	0.125	2.000	~287 °C for 2 h	0.0470	0.13
8	0.500	2.000	~287 °C for 2 h	0.0908	0.25
9	1.000	2.000	~287 °C for 2 h	0.1274	0.34

**Fig. 2** Powder X-ray diffractogram of the Mn_{0.34}Fe_{2.66}O₄ NPs, JCPDS card (19-0629) data for magnetite, and JCPDS card (10-0319) data for Jacobsite.

Colloidal stability under physiological conditions is one of the most important issues relating to the biomedical applications of nanomaterials. The synthesized MFNPs ($x = 0-0.34$) can be readily dispersed in H₂O or PBS without further surface modification. Dynamic light scattering (DLS) measurement of the Mn_{0.34}Fe_{2.66}O₄ NPs in PBS showed that their hydrodynamic size (D_H) was 8.2 nm, indicating that no particle aggregation in aqueous solution (see ESI, Fig. S2[†]). To investigate the effects of pH and ionic strength on the colloidal stability of the MFNPs, we exposed Mn_{0.34}Fe_{2.66}O₄ NPs to 0–1 M NaCl and pH 3–11 solutions, as shown in Fig. 3(a–d). The NPs are stable in NaCl solution at concentrations as high as 1 M, and stable over a pH range of 7–11. The solutions at pH 3 and pH 5 become almost colorless after placed for one week, due to the digestion of the NPs under acidic conditions. The colloidal stability of the NPs was further investigated by measuring D_H in PBS, NaCl solutions, and at several pH levels. The D_H results at 0 day and after placement for one week are shown in Fig. 3(e and f). The D_H values of the Mn_{0.34}Fe_{2.66}O₄ NPs are similar under various conditions and present an excellent stability for one week. The D_H results demonstrate that the Mn_{0.34}Fe_{2.66}O₄ NPs prepared by our procedure show excellent colloidal stability, which is promising for biomedical applications.

The excellent colloidal stability of the MFNPs in aqueous solutions indicates that PEG has been modified on the NP surface, and therefore the PEG can stabilize the NPs in a wide pH range due to the hydrogen bonding between PEG and water.³⁹ To confirm the surface chemical structure of the MFNPs, we collected the Fourier transform infrared (FTIR) spectra of the MFNPs. Fig. 4 shows the FTIR spectra of the Mn_{0.34}Fe_{2.66}O₄ NPs, TEG and HOOC-PEG-COOH. The characteristic bands of HOOC-PEG-COOH at 1106 cm⁻¹ (C–O–C stretch) and 2875 cm⁻¹ (CH₂ stretch), TEG at 3421 cm⁻¹ (OH stretch) appear in the spectrum of the Mn_{0.34}Fe_{2.66}O₄ NPs, indicating that HOOC-PEG-COOH and TEG is present on the nanocrystal surfaces. This was further demonstrated by the TGA (thermogravimetric analysis) result (see ESI, Fig. S3[†]). The distinct spectral difference between HOOC-PEG-COOH and HOOC-PEG-COOH on the Mn_{0.34}Fe_{2.66}O₄ NPs is that the carbonyl band at 1751 cm⁻¹ for HOOC-PEG-COOH is shifted to

**Fig. 3** (a–d) Colloidal stability test of the Mn_{0.34}Fe_{2.66}O₄ NPs in PBS, NaCl solutions (a and b), and at several pH (c and d). (a and c) Solutions freshly prepared; (b and d) solutions placed for one week. (e and f) Hydrodynamic sizes of the Mn_{0.34}Fe_{2.66}O₄ NPs in PBS, NaCl solutions (e), and at several pH (f). (e1) PBS solution freshly prepared; (e2) PBS solution placed for one week; (e3) 0 M NaCl solution placed for one week; (e4) 1 M NaCl solution placed for one week; (f1) aqueous solution at pH 7 freshly prepared; (f2–4) aqueous solutions at pH 7 (f2), pH 9 (f3) and pH 11 (f4) placed for one week.

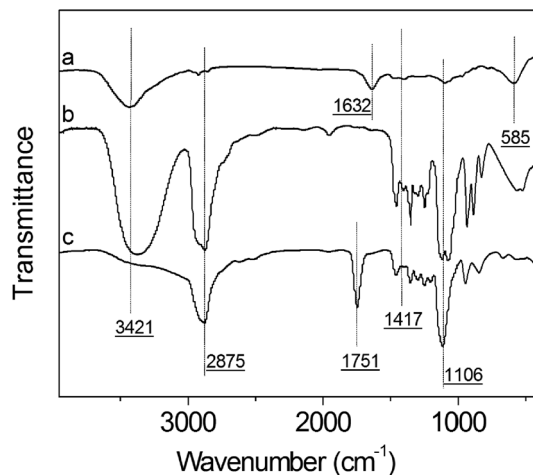


Fig. 4 FTIR spectra of (a) the Mn_{0.34}Fe_{2.66}O₄ NPs, (b) TEG and (c) HOOC-PEG-COOH.

a lower wavenumber, 1632 cm⁻¹ (COO⁻ asymmetric stretch), accompanied by the appearance of a new band at 1417 cm⁻¹ (COO⁻ symmetric stretch) when the HOOC-PEG-COOH was present on the Mn_{0.34}Fe_{2.66}O₄ NPs. This spectral change indicates that the carboxylate group in HOOC-PEG-COOH interacts with the metal on the nanocrystal surface and the carboxylic acid functionality has been transformed to carboxylate functionality.³⁹ In addition, the spectrum of the Mn_{0.34}Fe_{2.66}O₄ NPs exhibits characteristic peaks centered at 585 cm⁻¹ that are attributed to lattice absorption of the NPs.^{40–42}

The magnetic properties of the MFNPs were measured using a homemade vibrating sample magnetometer (VSM). Fig. 5 shows the magnetization loops of the MFNPs ($x = 0, 0.13, 0.25,$ and 0.34) measured at room temperature. All of the MFNPs exhibit superparamagnetic behavior without magnetic hysteresis and remanence. With the increase of 'x' value from 0, to 0.13, 0.25 and 0.34, the saturation magnetization of the MFNPs gradually increases.

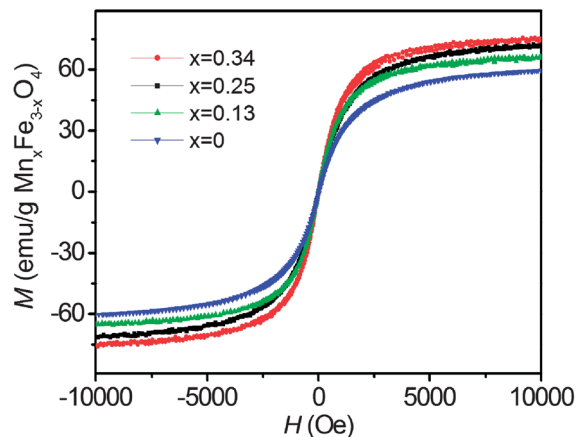


Fig. 5 Magnetization (M) loops for the MFNPs ($x = 0, 0.13, 0.25, 0.34$) measured at room temperature.

The saturation magnetizations of the Fe₃O₄ and Mn_{0.34}Fe_{2.66}O₄ NPs are 59.6 and 75.5 emu g⁻¹, respectively. Mn²⁺ is isoelectronic with Fe³⁺; so for small 'x', [Fe_{1-x}³⁺Mn_x²⁺](Fe_{1-x}²⁺Fe_{1+x}³⁺)O₄ gives a magnetic moment of (4 + x) μB (Bohr magneton) per formula unit.⁴³ This accounts for the increase of magnetic moment with Mn²⁺ substitution.

$T_1 + T_2$ dual-contrast agents require a high r_1 and a r_2 that is not significantly larger than r_1 . MR measurements were performed to evaluate the performance of the MFNPs as $T_1 + T_2$ dual-contrast agents. Fig. 6 shows the T_1 and T_2 -weighted MR images of the MFNPs ($x = 0, 0.13, 0.25,$ and 0.34) at different Fe + Mn concentrations (3 T, 25 °C). Increasing the concentration of the MFNPs led to a large decrease in signal intensity in the T_2 -weighted MR image. As a comparison, the commercial Magnevist didn't show obvious T_2 contrast effect, especially at low concentrations. With the increase of the 'x' value of the MFNPs, T_2 transverse relaxation rate increases. The r_2 values of the MFNPs, determined by calculating the slope of a plot of $1/T_2$

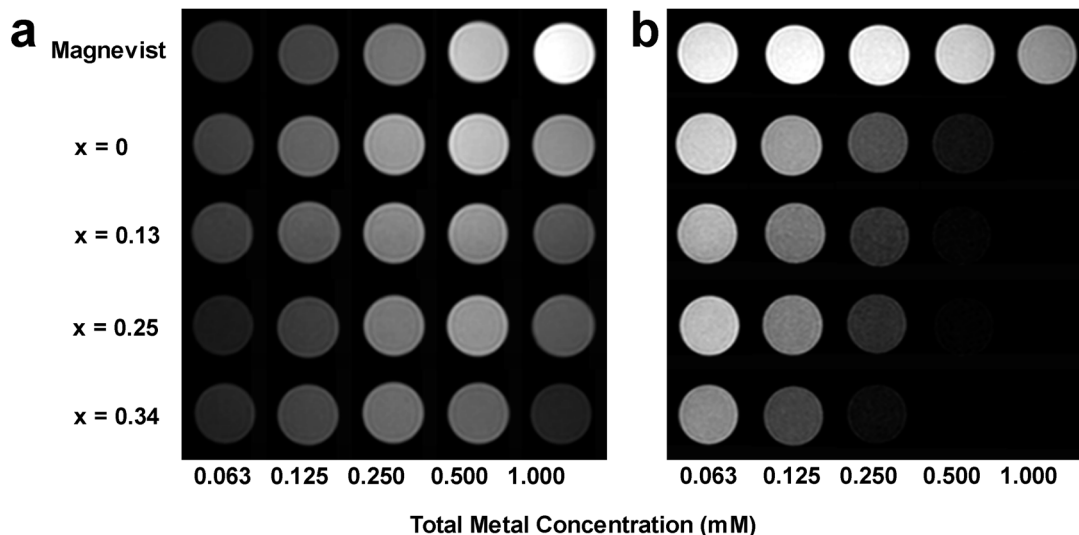


Fig. 6 (a) T_1 -weighted and (b) T_2 -weighted MR images of the aqueous solutions of the MFNPs ($x = 0, 0.13, 0.25, 0.34$) and Magnevist at different metal concentrations.

Table 2 Relaxivities of the MFNPs ($x = 0, 0.13, 0.25, 0.34$) at 1.5 T and 3 T

Sample	1.5 T			3 T		
	r_1 (mM ⁻¹ s ⁻¹)	r_2 (mM ⁻¹ s ⁻¹)	r_2/r_1	r_1 (mM ⁻¹ s ⁻¹)	r_2 (mM ⁻¹ s ⁻¹)	r_2/r_1
Fe ₃ O ₄	17.2	40.7	2.37	11.2	36.1	3.22
Mn _{0.13} Fe _{2.87} O ₄	19.3	53.9	2.79	10.6	49.7	4.69
Mn _{0.25} Fe _{2.75} O ₄	20.1	59.1	2.94	10.8	52.4	4.85
Mn _{0.34} Fe _{2.67} O ₄	21.5	67.2	3.13	10.5	66.8	6.36

versus Fe + Mn concentration, were shown in Table 2. The r_2 gradually increases as the Mn²⁺ doping amount of the MFNPs increases from $x = 0$ to 0.34. The T_1 contrast effects are more complicated than T_2 contrast effects. As the concentration of the MFNPs is below 0.250 mM, increasing concentration of the MFNPs led to an obvious increase in signal intensity in the T_1 -weighted MR image. Compared with commercial Magnevist, all the MFNPs ($x = 0, 0.13, 0.25, \text{ and } 0.34$) show better T_1 contrast effects. When the concentration of the MFNPs increases from 0.250 to 0.500 mM, the T_1 contrast effects of the MFNPs didn't show obvious change. Consequently, the Fe₃O₄ NPs show similar T_1 contrast effect with Magnevist; however, other MFNPs ($x = 0.13, 0.25, 0.34$) are not as good as Magnevist. As the concentration of the MFNPs is increased up to 1.000 mM, an unusual decrease in signal intensity were found in the T_1 -weighted MR image and resulted in much worse T_1 contrast effects of the MFNPs than Magnevist. This is due to the high T_2 contrast effects of the MFNPs. Therefore, to act as T_1 and T_2 dual contrast agents at 3 T, the concentration of the MFNPs need to be lower than 0.500 mM. As shown in Table 2, the r_1 values of the MFNPs ($x = 0, 0.13, 0.25, 0.34$) at 3 T are similar. However, due to the low r_2/r_1 ratio, Fe₃O₄ NPs present superior T_1 contrast effect than other three samples. The relaxation properties of the MFNPs ($x = 0, 0.13, 0.25, 0.34$) at 1.5 T were also investigated. T_1 and T_2 values of the MFNPs at different Fe + Mn concentrations were measured on a 1.5 T relaxometer at 37 °C. As shown in Table 2, the r_1 , r_2 , and r_2/r_1 gradually increase as the Mn²⁺ doping amount of the MFNPs increases from $x = 0$ to 0.34. The r_1 values of the MFNPs at 1.5 T are around twice of those at 3 T, however, the r_2 values at 1.5 T are a little increase than those at 3 T. Consequently, the r_2/r_1 ratios of the MFNPs at 1.5 T are much lower than those at 3 T, indicating superior T_1 and T_2 dual MR contrast effects at 1.5 T.

4. Conclusions

In summary, a facile one-pot reaction was developed to synthesize water-soluble, PEG-coated MFNPs. The 'x' value could be effectively tuned from 0 to 0.34 through adjusting the reaction conditions, including reaction time, metal precursor concentration and heating procedure. The produced MFNPs could be individually dispersed in physiological buffer with high stability, which is an important guarantee for their biomedical applications. With the increase of the 'x' value of the MFNPs, T_2 contrast effects are enhanced while T_1 contrast effects are weakened. The T_1 contrast effects of the MFNPs are

concentration dependant and they could act as good T_1 and T_2 dual contrast agents when their concentration is lower than 0.500 mM at a magnetic field strength of 3 T. Due to their excellent colloidal stability under physiological conditions and good performance in MRI, the MFNPs should have great potential for molecular imaging and diagnostic applications.

Acknowledgements

We thank Dr Meihong Du for the relaxation time measurements. This work was supported by the Natural Science Foundation of China (no. 21103012 and 21273022), SRF for ROCS, SEM, the Fundamental Research Funds for the Central Universities, and Beijing National Laboratory for Molecular Sciences open research fund.

Notes and references

- 1 J. W. M. Bulte and D. L. Kraitchman, *NMR Biomed.*, 2004, **17**, 484–499.
- 2 T. Schroeder, *Nature*, 2008, **453**, 345–351.
- 3 H. R. Herschman, *Science*, 2003, **302**, 605–608.
- 4 R. Weissleder and U. Mahmood, *Radiology*, 2001, **219**, 316–333.
- 5 F. Hu, L. Wei, Z. Zhou, Y. Ran, Z. Li and M. Gao, *Adv. Mater.*, 2006, **18**, 2553–2556.
- 6 C. Wilhelm and F. Gazeau, *Biomaterials*, 2008, **29**, 3161–3174.
- 7 C. T. Yavuz, J. T. Mayo, W. W. Yu, A. Prakash, J. C. Falkner, S. Yean, L. Cong, H. J. Shipley, A. Kan, M. Tomson, D. Natelson and V. L. Colvin, *Science*, 2006, **314**, 964–967.
- 8 X. Bai, S. J. Son, S. Zhang, W. Liu, E. K. Jordan, J. A. Frank, T. Venkatesan and S. B. Lee, *Nanomedicine*, 2008, **3**, 163–174.
- 9 E. J. W. Verwey, *Nature*, 1939, **144**, 327–328.
- 10 F. Hu, K. W. MacRenaris, E. A. Waters, T. Liang, E. A. Schultz-Sikma, A. L. Eckermann and T. J. Meade, *J. Phys. Chem. C*, 2009, **113**, 20855–20860.
- 11 F. Hu, K. W. MacRenaris, E. A. Waters, E. A. Schultz-Sikma, A. L. Eckermann and T. J. Meade, *Chem. Commun.*, 2010, **46**, 73–75.
- 12 S. H. Sun, H. Zeng, D. B. Robinson, S. Raoux, P. M. Rice, S. X. Wang and G. X. Li, *J. Am. Chem. Soc.*, 2004, **126**, 273–279.
- 13 J.-t. Jang, H. Nah, J.-H. Lee, S. H. Moon, M. G. Kim and J. Cheon, *Angew. Chem., Int. Ed.*, 2009, **48**, 1234–1238.

- 14 J.-H. Lee, Y.-M. Huh, Y.-w. Jun, J.-w. Seo, J.-t. Jang, H.-T. Song, S. Kim, E.-J. Cho, H.-G. Yoon, J.-S. Suh and J. Cheon, *Nat. Med.*, 2007, **13**, 95–99.
- 15 F. Liu, S. Laurent, H. Fattahi, L. V. Elst and R. N. Muller, *Nanomedicine*, 2011, **6**, 519–528.
- 16 C. Barcena, A. K. Sra, G. S. Chaubey, C. Khemtong, J. P. Liu and J. Gao, *Chem. Commun.*, 2008, 2224–2226.
- 17 U. I. Tromsdorf, N. C. Bigall, M. G. Kaul, O. T. Bruns, M. S. Nikolic, B. Mollwitz, R. A. Sperling, R. Reimer, H. Hohenberg, W. J. Parak, S. Forster, U. Beisiegel, G. Adam and H. Weller, *Nano Lett.*, 2007, **7**, 2422–2427.
- 18 F. Hu and Y. S. Zhao, *Nanoscale*, 2012, **4**, 6235–6243.
- 19 F. Hu, Q. Jia, Y. Li and M. Gao, *Nanotechnology*, 2011, **22**, 245604.
- 20 E. Taboada, E. Rodriguez, A. Roig, J. Oro, A. Roch and R. N. Muller, *Langmuir*, 2007, **23**, 4583–4588.
- 21 U. I. Tromsdorf, O. T. Bruns, S. C. Salmen, U. Beisiegel and H. Weller, *Nano Lett.*, 2009, **9**, 4434–4440.
- 22 J. Y. Park, P. Daksha, G. H. Lee, S. Woo and Y. M. Chang, *Nanotechnology*, 2008, **19**, 365603–365609.
- 23 L. Zeng, W. Ren, J. Zheng, P. Cui and A. Wu, *Phys. Chem. Chem. Phys.*, 2012, **14**, 2631–2636.
- 24 B. H. Kim, N. Lee, H. Kim, K. An, Y. I. Park, Y. Choi, K. Shin, Y. Lee, S. G. Kwon, H. B. Na, J.-G. Park, T.-Y. Ahn, Y.-W. Kim, W. K. Moon, S. H. Choi and T. Hyeon, *J. Am. Chem. Soc.*, 2011, **133**, 12624–12631.
- 25 L. Zeng, W. Ren, J. Zheng, A. Wu and P. Cui, *Appl. Surf. Sci.*, 2012, **258**, 2570–2575.
- 26 C. Y. Shu, F. D. Corwin, J. F. Zhang, Z. J. Chen, J. E. Reid, M. H. Sun, W. Xu, J. H. Sim, C. R. Wang, P. P. Fatouros, A. R. Esker, H. W. Gibson and H. C. Dorn, *Bioconjugate Chem.*, 2009, **20**, 1186–1193.
- 27 Z. Li, P. W. Yi, Q. Sun, H. Lei, H. L. Zhao, Z. H. Zhu, S. C. Smith, M. B. Lan and G. Q. Lu, *Adv. Funct. Mater.*, 2012, **22**, 2387–2393.
- 28 A. Boni, M. Marinone, C. Innocenti, C. Sangregorio, M. Corti, A. Lascialfari, M. Mariani, F. Orsini, G. Poletti and M. F. Casula, *J. Phys. D: Appl. Phys.*, 2008, **41**, 134021.
- 29 D.-H. Kim, H. Zeng, T. C. Ng and C. S. Brazel, *J. Magn. Magn. Mater.*, 2009, **321**, 3899–3904.
- 30 H. Hu, Z.-q. Tian, J. Liang, H. Yang, A.-t. Dai, L. An, H.-x. Wu and S.-p. Yang, *Nanotechnology*, 2011, **22**, 085707.
- 31 N. Bao, L. Shen, Y. Wang, P. Padhan and A. Gupta, *J. Am. Chem. Soc.*, 2007, **129**, 12374–12375.
- 32 U. I. Tromsdorf, N. C. Bigall, M. G. Kaul, O. T. Bruns, M. S. Nikolic, B. Mollwitz, R. A. Sperling, R. Reimer, H. Hohenberg, W. J. Parak, S. Forster, U. Beisiegel, G. Adam and H. Weller, *Nano Lett.*, 2007, **7**, 2422–2427.
- 33 H. B. Na, I. C. Song and T. Hyeon, *Adv. Mater.*, 2009, **21**, 2133–2148.
- 34 J. Lu, S. Ma, J. Sun, C. Xia, C. Liu, Z. Wang, X. Zhao, F. Gao, Q. Gong, B. Song, X. Shuai, H. Ai and Z. Gu, *Biomaterials*, 2009, **30**, 2919–2928.
- 35 F. Y. Cheng, C. H. Su, Y. S. Yang, C. S. Yeh, C. Y. Tsai, C. L. Wu, M. T. Wu and D. B. Shieh, *Biomaterials*, 2005, **26**, 729–738.
- 36 Q. Song, Y. Ding, Z. L. Wang and Z. J. Zhang, *Chem. Mater.*, 2007, **19**, 4633–4638.
- 37 E. Kang, J. Park, Y. Hwang, M. Kang, J. G. Park and T. Hyeon, *J. Phys. Chem. B*, 2004, **108**, 13932–13935.
- 38 H. Yang, C. Zhang, X. Shi, H. Hu, X. Du, Y. Fang, Y. Ma, H. Wu and S. Yang, *Biomaterials*, 2010, **31**, 3667–3673.
- 39 Q. Liu and Z. Xu, *Langmuir*, 1995, **11**, 4617–4622.
- 40 Y. W. Jun, Y. M. Huh, J. S. Choi, J. H. Lee, H. T. Song, S. Kim, S. Yoon, K. S. Kim, J. S. Shin, J. S. Suh and J. Cheon, *J. Am. Chem. Soc.*, 2005, **127**, 5732–5733.
- 41 F. Q. Hu, Z. Li, C. F. Tu and M. Y. Gao, *J. Colloid Interface Sci.*, 2007, **311**, 469–474.
- 42 P. Tartaj, M. D. Morales, S. Veintemillas-Verdaguer, T. Gonzalez-Carretero and C. J. Serna, *J. Phys. D: Appl. Phys.*, 2003, **36**, R182–R197.
- 43 J. Giri, P. Pradhan, V. Somani, H. Chelawat, S. Chhatre, R. Banerjee and D. Bahadur, *J. Magn. Magn. Mater.*, 2008, **320**, 724–730.